International Journal of Engineering Trends and Technology
ISSN: 2231 – 5381 /doi:10.14445/22315381/IJETT-V70I3P223

Volume 70 Issue 3, 201-211, March 2022

Original Article

A Novel RGB Channel Assimilation for Hyperspectral Image Classification using 3D-Convolutional Neural Network with Bi-Long Short-Term Memory

M. Preethi[1], C. Velayutham[2], S. Arumugaperumal[3]

[1] *Research Scholar (Reg. No: 17224012162073), Department of Computer Science, S.T. Hindu College, Nagercoil, Affiliated to Manonmaniam Sundaranar University, Tamil Nadu, India.*
[2] *Associate Professor & Head, Department of Computer Science, Aditanar College, Tiruchendur, TamilNadu, India.*
[3]*Head, Department of Computer Science, S.T. Hindu College, Nagercoil, TamilNadu, India.*

[1]preethiindira12@gmail.com, [2]cvsir22@yahoo.com,[3] visvenk@yahoo.co.in

Abstract — *Hyperspectral image (HSI) contains high dimensionality of spectral information, which is not easy to classify every pixel. To confront the problem, we propose a novel RGB channel Assimilation for classification methods. This work discusses the classification of hyperspectral images based on Domain Transform Interpolated Convolution Filter (DTICF) and 3D-CNN with Bi-directional-Long Short Term Memory (Bi-LSTM). Before using the DTICF, the RGB images of HSI and the patch of the input image from raw HSI are integrated. Those obtained spatial and spectral features are finally given into the designed 3D-CNN with the Bi-LSTM framework. The excerpted colour features are classified by 2D-CNN. The probabilistic classification map of 3D-CNN-Bi-LSTM and 2D-CNN are fused. In the last step, additionally, Markov Random Field (MRF) is utilized for improving the fused probabilistic classification map. Based on the experimental results, two different hyperspectral images prove that novel RGB channel assimilation of DTICF-3D-CNN-Bi-LSTM provides good classification results.*

Keywords — *Bi directional-Long Short Term Memory, Deep Learning, Domain Transform Interpolated Convolution Filter.*

I. INTRODUCTION

Normal RGB image has bands of bands such as red, green, and blue, but HSI has several bands. For example, HSI contains three dimensions. The first two dimensions of the height and width are spatial (x, y-axis), while the third dimension of the spectral (z-axis) is the wavelength. Wavelength is acquired by electromagnetic spectrum [17]. The human eyes see colour over wavelength ranging roughly from 400 nm (violet) to 700nm (red) but wavelength range from 700nm-2500nm in HSI. HSI contains continuous spectral bands which are procured by hyperspectral sensors. There are many applications used in HSI, such as medical imaging, microscopy or endoscopy, precision agriculture, mineralogy, and food inspection. Many researchers commonly used machine learning and deep learning methods for hyperspectral images. However, HSI is more difficult compared to the normal RGB image. In the last few years, many HSI classification methods have been proposed [7], [9], such as spectral-based approaches and spectral-spatial-based approaches [31]. Spectral features are first extracted by some feature extraction methods [4], such as Principal Component Analysis (PCA) [5], Independent Component Analysis (ICA) [18], and Linear Discriminant Analysis (LCA) [1]. Then, the obtained features are applied to learn the classifier [3]. In spectral-spatial-based methods, texture features [14] and structure features [6] are extracted and combined by utilizing composite kernels [11]. However, the obtained features are hand-crafted.

Recently [3], [23-24], many researchers utilized a deep learning approach for image processing such as image classification [33], image segmentation [21] and object detection [34]. Among deep approaches, CNN [12] has been utilized for capturing the features of spectral and spatial for HSI classification. Yushi Chen et al. [35] introduced the deep learning concept for HSI classification for the first time. Konstantinos Makantasis et al. [16] utilized deep learning methods for the HSI classification method, which exploits features using CNN and this work utilized a Multi-Layer Perceptron for a classification task. Shaohui Mei et al. [30] introduced new classification techniques, namely a novel five-layer CNN such as batch normalization, dropout, Parametric Rectified Linear Unit (PReLu) activation function. Spatial context and spectral information are elegantly integrated into the framework that is used to extract the features. Haokui Zhang et al. [8] proposed an end-to-end

3-D lightweight CNN which has a deeper network structure, fewer parameters, and lower computation cost, resulting in better classification performance. Qin Xu et al. [28] designed multiscale convolution from 3D-CNN, which is used to obtain the pair of spectral-spatial features and also reduce the spatial redundancy. Radhesyam Vaddi et al. [29] proposed new classification techniques based on data normalization and CNN. In this work, Probabilistic Principal Component Analysis (PPCA) and Gabor filtering are used for obtaining the features which are used to reduce the computational time. In Jia et al. [13], a 3-dimensional (3-D) Gabor-wavelet was developed for hyperspectral classification. It helps to predict the features via 3-D. Kang et al. [15] acquired the spectral features by Gabor filtering to form the fused features for Gabor filtering-based deep network (GFDN). In particular, CLSTM is used for obtaining the spectral features of HSIs, which improve the extraction of spatial features using convolutional operators [32].

The main contributions are stated below: Compared with machine learning techniques, Deep learning methods obtain good performance for HSI classification.

- We propose a novel RGB channel Assimilation for colour classification methods. The RGB colour space is the most efficient colour representation method on HSI classification.
- Additionally, we have introduced a new HSI classification framework. This framework is analyzed how to integrate the Domain Transform Interpolated Convolution Filter (DTICF) and 3D-CNN with BiLSTM.
- The proposed method is divided into two processing:
- In the First processing, HSI data is converted to RGB image.
- RGB image and patch-wise input image with spectral information are integrated.
- Then, the excerpted features of spectral and spatial are obtained using DTICF by RGB image with spatial features and spectral bands from HSI data.
- The excerpted features are provided in the 3D-CNN framework.
- The extracted deep features are again fed in the Bi-LSTM network.
- In the second step, the colour features are extracted using chromaticity computation, and extracted features are classified by 2D-CNN.
- The probabilistic classification map of 3D-CNN-Bi-LSTM and 2D-CNN is fused.
- Finally, additionally, Markov Random Field (MRF) is utilized for improving the fused probabilistic classification map efficiently. The proposed novel RGB channel Assimilation of DTICF-3D-CNN-BiLSTM-MRF shows good classification accuracy with low computational time.

The paper is assembled in the following ways. Proposed methods are debated in section 2. The methodology is reported in section 3. The technical description is delineated in Section 4. The experimental results for the proposed method are elucidated in section 5. Section 6 is presented with the conclusion.

II. PROPOSED METHOD

In this portion, the proposed novel RGB Channel Assimilation of DTICF-3D-CNN-Bi-LSTM HSI classification is discussed. First, the HSI data is converted to an RGB image with spatial features. RGB images with spatial features are converted to grey-level images. These spatial-based features are integrated with patch-wise input data from HSI images. Further, the patch-wise spectral-spatial features are acquired using DTICF by a grey level image with spatial and spectral bands. The hyperspectral data with features is provided to newly developed 3D-CNN architecture for classification. In this section, 3D-CNN with Bi-LSTM based classification method is explained and discusses how to train the network with deep learned features from HSI. 3D-CNN configuration substantially consists of three blocks of Convolution (c_1, c_2, c_3) and ReLU (R_1, R_2, R_3) layers. The filters used in three sets are k_1 = 20, k_2= 20 and k_3 = 35 respectively.

The extracted features of the HSI $(x_1, y_1, 1)$ are given as input to 3D_CNN. In 3D-CNN, the first convolutional layer c_1 with k_1 filters data becomes (x_1, y_1, k_1) and (x_2, y_2, k_1). In the second convolutional layer, c_2 with k_2 filters, the data becomes (x_2, y_2, k_2). and (x_3, y_3, k_2). Finally, we obtain the data (x_3, y_3, k_3) by using the third set of Convolution and ReLU layers. The ReLU features are given into the Bi-LSTM network to extract features. In the last stage of the Bi-LSTM model, we take the input of the ReLU features obtained by 3D-CNN. The final data is categorized by applying a soft-max function. At the same proposed architecture, RGB images with spatial features are classified using 2D-CNN. The probability map of 3D-CNN with Bi-LSTM and 2D-CNN is fused. The fused probability map can also be improved by MRF efficiently.

III. METHODOLOGY

A. RGB Channel Assimilation

The proposed RGB channel assimilation is the most efficient classification method. The RGB images are produced by a digital representation which is categorized by the intensity value of a pixel. The 3-dimensional vector is calculated by intensity value. RGB colour space is utilized for image display. All camera, printer, or other devices provides direct RGB signal as input and output. The transformation of RGB space is proposed for extracting efficient colour features. The RGB space is computed by RGB chromaticity value which yields higher classification accuracy than the direct use of R, G, and B value.

B. Computation of chromaticity

In RGB space, the chromaticity value is calculated for chromaticity coordinates. The chromaticity coordinates are the average value of RGB colour space. Fig 1 shows the structure of RGB channel Assimilation and summarizes the RGB colour space in algorithm 1.

$$r(R, G, B)= R, \frac{G+R}{2}, \frac{B+R}{2} \tag{1}$$

$$g(G, R, B)= G, \frac{R+G}{2}, \frac{B+G}{2} \tag{2}$$

$$b(B, G, R)= B, \frac{G+B}{2}, \frac{R+B}{2} \tag{3}$$

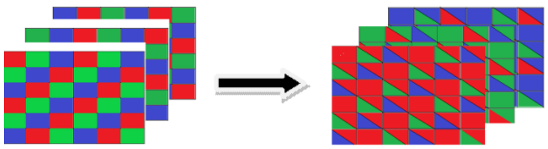

Fig. 1 Structure of RGB channel Assimilation

Algorithm 1: RGB Channel Assimilation for HSI Classification

Input: HSI data H $\in R^{h\times w\times d}$, Number of diagonal value K

Output: RGB channel Patches

1. Set rpatch to Red channels;
2. Set gpatch to Green channels;
3. Set bpatch to Blue channels;
4. For diagonal value is 5 % Red channels
5. If k is equal to 1
6. Set fm to rpatch;
7. Set sm to rpatch;
8. Elseif k is equal to 2
9. Set fm to rpatch;
10. Set sm to gpatch;
11. Elseif k is equal to 3
12. Set fm to rpatch;
13. Set sm to bpatch;
14. Elseif k is equal to 4
15. Set fm to rpatch;
16. Set sm to rpatch;
17. Elseif k is equal to 5
18. Set fm to rpatch;
19. Set sm to gpatch;
20. End if
21. End for
22. Initialize j to one;
23. For i=k-1:1
24. Rpatch(i,j)=(fm(i,j)+sm(i,j))/2.0;
25. j= j+1;
26. End for
27. Repeat step 4 to 26 for Green and Blue Channels

C. Domain Transform Interpolated Convolution Filter (DTICF)

DTICF was proposed by Oliveria [27] for image filtering, which utilizes for enhancing spatial features. It is a spatially invariant feature and is used to decrease the pixel distance. If any find the distance between the pixel, we have to use the spatially invariant performance. It is the edge-preserving filter. It is calculated in the following ways:

$$Z_i(u) = \int_{\Omega_w} P_w Q(h(u), x)dx \;\; i = 1,2, \dots, n; u \in \Omega_w \tag{4}$$

In Equation (1) [27], Filtering P_w is evaluated by the consecutive convolution, where Q is a normalized box kernel, and r is the filter radius.

$$Q(h(u), x) = \frac{1}{2r}\delta\{|g(u) - x| \le r\} \tag{5}$$

$$(E)=\begin{cases}1 & E \text{ is true} \\ 0 & other\end{cases} \tag{6}$$

Substituting Equations (5), [27] and (6) into (4):

$$F_i(u) = \frac{1}{2r}\int_{g(u)-r}^{g(u)+r} P_w(x)dx \tag{7}$$

$$G(u)=\int_0^u 1 + \frac{\sigma_s}{\sigma_r}\sum_{i=1}^{c} |I'_k(x)dx| \tag{8}$$

$$\sigma_r = \sqrt{3\sigma_j} \tag{9}$$

$$\sigma_{jn} = \sigma_s\sqrt{3}\frac{2^{M-n}}{\sqrt{4^M - 1}} \tag{10}$$

D. CNN Operation

Nowadays, many researchers utilize the deep learning method for image classification for excellent performance [5]. CNN is employed to capture the spatial and temporal dependencies in the input image. This algorithm is used for the image data set due to the reduction of dimensionality. CNN doesn't care about the large size of data, but it is manipulated to perceive the parameters of the image.

E. 3D Convolution

3D-CNN is employed to extract the features of spatial and spectral information simultaneously. In 3D data cube, 3D convolution is computed by the weighted sum of pixels as:

$$C_{pqr}=f\,(\textstyle\sum_{i,j,k} w_{ijk}\, a_{(p+i)(q+j)(r+k)}+b) \tag{11}$$

F. Bi-Long Short Term Memory (BILSTM)

Bi-LSTM network LSTM was established by Hochreiter and Schmidedhuber [10]. This network structure overcomes the problems of RNN [25]. In Bi-LSTM, there are three memory gates such as input, forget and output. The high-frequency Intrinsic Mode Function (IMF) is C_{ash} that is given as input, and h_{i-1} is the output. CS_{T-1} is the input of cell state determined by forgetting gate f_t using a sigmoid function. It is written in Eq. 10 [10]:

$$f_t = (w_f[h_{i-1}, C_{tsh}] + b_f) \quad (12)$$

Input gate i_t is used to determine the values that are to be updated to CS_t as in Eq. 12 [10]:

$$i_t = (w_i[h_{i-1}, C_{tsh}] + b_i) \quad (13)$$

The output gate o_t are equated in Eq. 13 [10]:

$$Cs_t = f_i \odot CS_{t-1} \oplus i_t \odot CS_{t-1} \quad (14)$$

Consequently, the output of LSTM memory cell is written in Eq. 14[10]:

$$h_N = o_t \odot Cs_t \quad (15)$$

$$y_d = \text{softmax}(W_o \cdot h_N. + b_o) \quad (16)$$

IV. HSI CLASSIFICATION WITH DTICF-3D-CNN-BILSTM-MRF

In this portion, the proposed method DTICF-3D-CNN-BiLSTM-MRFis was discussed. First, HSI data is converted to RGB image and RGB image with spatial features and spectral information with original HSI is integrated. DTICF is applied in integrated information.

Those obtained spatial and spectral features are finally given into the designed 3D-CNN-BiLSTM framework. The proposed method is discussed in Fig. 2.

A. Extracting Spatial Features by DTICF

First, we convert the HSI image into an RGB image. Then, DTICF is applied to RGB images with spatial and spectral bands from original HSI Data. For dataset $D = \{d_1, d_2, .. d_s\}$, we utilized the DTICF to capture the features.

$$[g_1, g_2, .., g_s] = \text{RGB (D)} \quad (17)$$

B. Classifying HSI by 3D-CNN-Bi-LSTM

We obtain the image $U = \{u_1, u_2, ..., u_s\}$ by DTICF filter. In the proposed method, a 3D-CNN network is utilized to obtain the pair features of spectral-spatial using convolution, pooling and ReLU layers. Using Equation (8), the extracted features of the HSI (x_1, y_1, 1) is given as input to 3D_CNN. In 3D-CNN, first convolutional layer c_1 with k_1 filters data becomes (x_1, y_1, k_1) and (x_2, y_2, k_1). In the second convolutional layer, c_2 with k_2 filters, the data becomes (x_2, y_2, k_2). and (x_3, y_3, k_2). Finally, we obtain the data (x_3, y_3, k_3) by using the third set of Convolution and ReLU layers. Finally, we obtain the spectral-spatial features by ReLU. BiLSTM is applied to extract the sequence features from 3D-CNN. Next, a dropout layer is used to avoid over-fitting. Then, we adopt a soft-max function for classifying the entire feature vector. Eventually, the 3D-CNN network provides the probabilistic classification map C.

C. Fused DTICF-3D-CNN-BiLSTM and RGB Channel Assimilation 2D-CNN

In the beginning, the probability classification map $c = \{p_1, p_2, ..., p_n\}$ is defined and the number of categories is defined by n for classifying. Then we applied 2D-CNN using Equation (8) to RGB images with spatial features. The probability map of 3D-CNN-BiLSTM and RGB channel assimilation 2D-CNN are fused. Finally, MRF is utilized for enhancing the fused probabilistic classification map.

The proposed method analyzes the output by using log-likelihood log $P((y_i|\tilde{y}_i)$ can be given by [11]

$$\hat{y} = \arg\max_{y \in K^n} \left\{ \sum_{i=1}^{n} \sum_{k=1}^{K} 1\{y_i = k\} \log \tilde{y}_{ik} + \mu \sum_{i=1}^{n} \sum_{j \in N(i)} \delta(y_i - y_j) \right\} \quad (18)$$

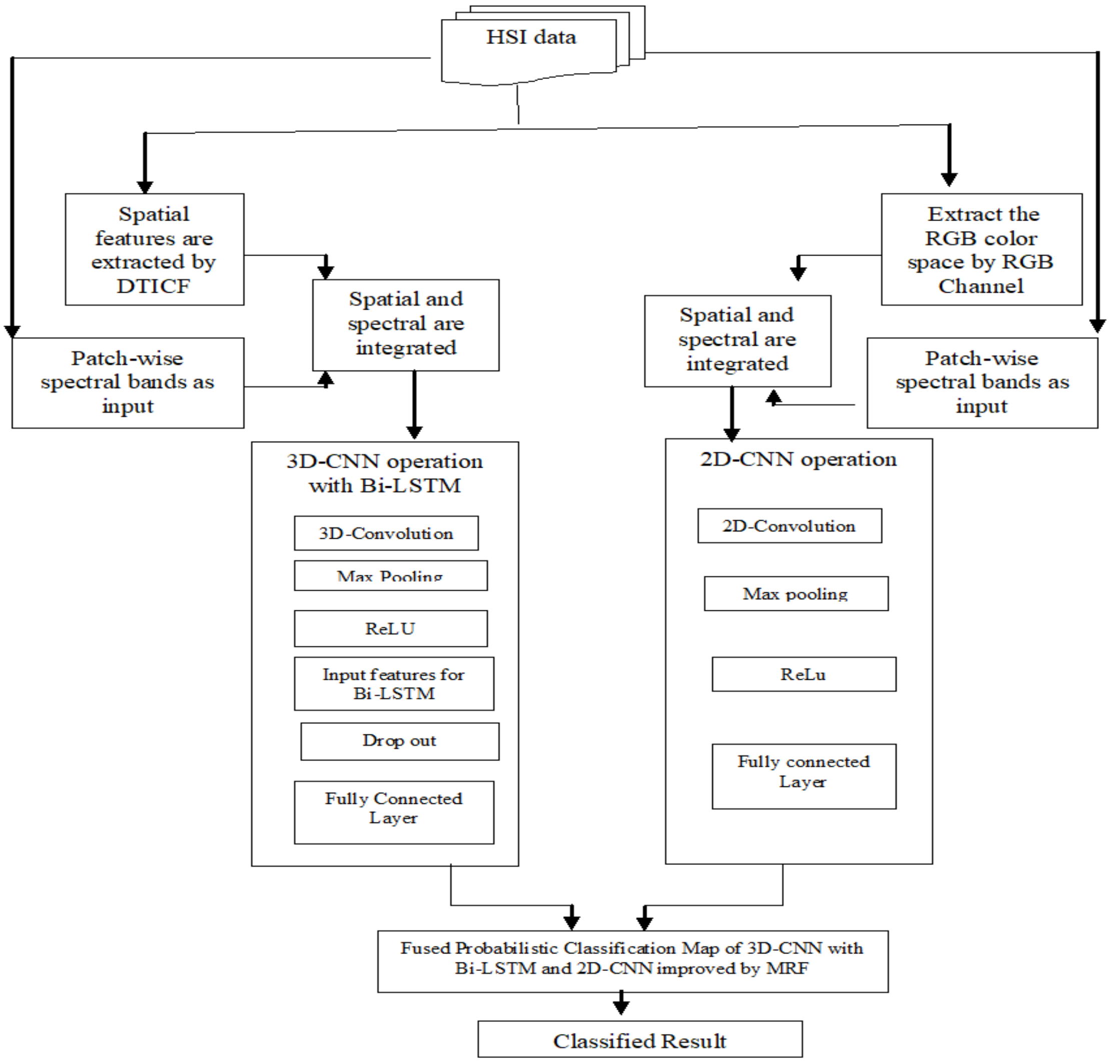

Fig. 2 HSI Classification procedure

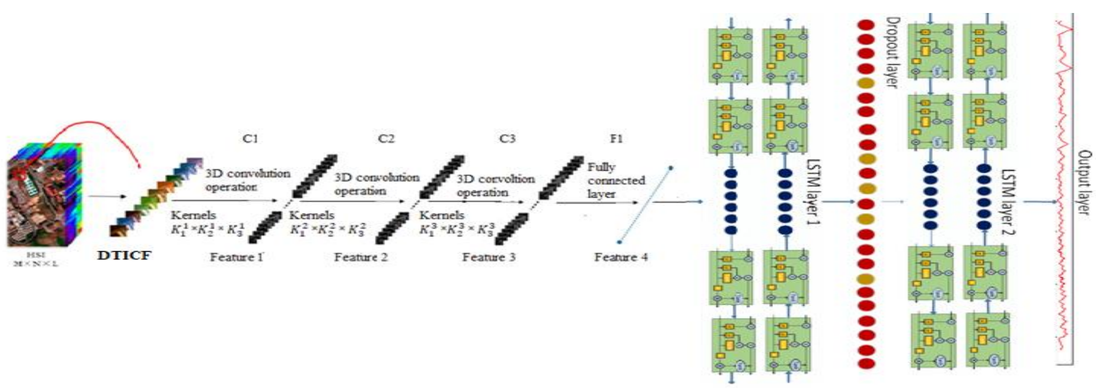

Fig. 3 Network Structure of DTICF-3D-CNN-Bi-LSTM

Algorithm 2: RGB Channel Assimilation of Hyperspectral Image Classification

Input: HSI data H $\in R^{h\times w\times d}$, D for Training Data, patches y = $\{y_1, y_2, \ldots, y_n\}$, K for number of labels.

Output: Labels $\hat{y}$.

1. For Each patches $x_i, \in R^{k\times k\times d}$ in H, do
2. Obtain spectral-spatial feature through DTICF using Eq. (4);
3. X = $\{x_1, x_2, \ldots, x_n\}$;
4. While D: 1 → X
5. Compute the patch for training data;
6. Compute another patch for testing;
7. $D_{l(k)}^{(k)} = \{(x_1, y_1), \ldots, (x_{l(k)}, y_{l(k)})\}$;
8. Generate feature maps operation using convolutionoperation Eq. (11) ;
9. f(x) = max (0,x); % ReLU operation
10. Sequence input by f(x) given Bi-LSTM network using Eq. (12);
11. Perform forward and backward sequence using Eq. (15) to generate the feature;
12. Compute a = $\frac{\exp(o)}{\sum_k \exp(o_k)}$; % Soft-max activation function
13. end while
14. compute RGB channel assimilation patches;
15. Obtain spectral-spatial feature through 2D-CNN;
16. end for
17. compute probabilistic classification map for 3D-CNN-BiLSTM and 2D-CNN
18. Compute the classifiaction label $\hat{y}$ using Eq. (18).

V. EXPERIMENTS

In this portion, the proposed RGB Channel Assimilation of DTICF-3D-CNN-BiLSTM-MRF is examined in two hyperspectral data set, such as Indian pines data and Pavia University data. The experimentations are carried out on Matlab R2019a on a PC with 64 GB RAM. There are three measurements used for validation such as [1]: Overall accuracy (OA), Average Accuracy (AA), and Statistically kappa measure (k).

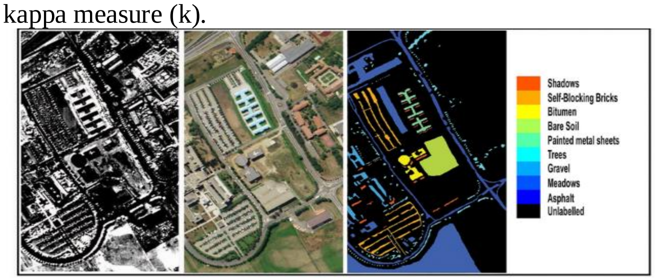

Fig. 4 Original image and Ground Truth of Pavia University dataset

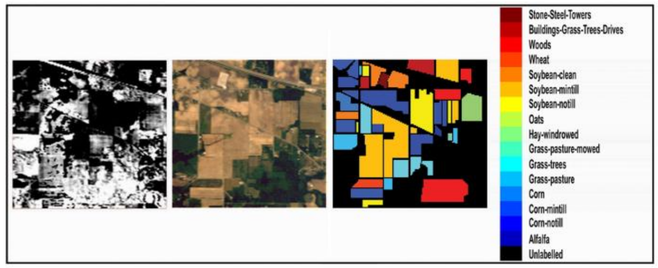

Fig. 5 Original image and Ground Truth of Indian Pines dataset

In this portion, the Indian pines data set was acquired by an Airborne Visible/Infrared Imaging Spectrometer (AVIRIS) sensor. It defines the spatial dimension size of height and width as 145×145. It contains 220 spectral reflectance bands, and it is measured by wavelength range 0.4–2.5 μm.

It contains 16 classes and is displayed in figure 4. Pavia University dataset was accumulated by the Reflective Optics System Imaging Spectrometer (ROSIS) over the urban area of the University of Pavia, northern Italy. It defines the spatial dimension size of height and width 610×340. It contains 103 spectral bands. There are 9 land cover classes in this dataset, and the number of each class is displayed in figure 5.

A. The proposed RGB Channel Assimilation of DTICF-3D-CNN-BiLSTM-MRF HSI Classification on Indian pines data and Pavia University data

To examine the proposed RGB Channel Assimilation of DTICF-3D-CNN-MRF, we select 50% of samples for training data and then another 50% of samples for testing. In this experiment, 3D-CNN-BiLSTM architecture is structured as follows (also shown in Table I), and validation accuracy is also displayed in Table II.

Table 1. The network structure of the proposed method in the Indian pines dataset

Input Shape	Function	Output shape
3D-CNN	image3dInputLayer([5 5 200 1],"Name","image3dinput")	
(5×5×3)	convolution3dLayer([3 3 3],20, "Name","conv1","Stride",[1 1 1],"Padding",[0 0 1;0 0 1])	(3×3×20)
(3×3×20)	Activation = ReLU	(3×3×20)
(3×3×20)	convolution3dLayer([1 1 3],20, "Name","conv2","Stride",[1 1 2],"Padding",[0 0 1;0 0 1])	(3×3×20)
(3×3×20)	Activation = ReLU	(3×3×20)

(3×3×20)	convolution3dLayer([3 3 3],35, "Name","conv3","Stride",[1 1 1],"Padding",[0 0 1;0 0 1])	(3×3×35)
(3×3×35)	convolution3dLayer([1 1 3],35, "Name","conv4","Stride",[1 1 2],"Padding",[0 0 1;0 0 1])	(1×1×35)
(1×1×35)	Activation = ReLU	(1×1×35)
(1×1×35)	Fully Connected Layer	1×1×910 Weights 540×35 Bias 540 ×1
1×1×540	Activation = ReLU 1×1×540	1×1×540
BiLSTM		
540	Dense 1 540 (input layer) Activation=ReLU Sequence input with 540 dimension	540
540	BiLSTM 1 with 512 hidden units	1024 Input Weights (4096)
1024	Dropout 50%	1024
1024	BiLSTM 2 with 256 hidden units	512 Input Weights (2048)
512	Dropout 50%	512
512	Fully Connected Layer 9	Weight 9×512 Bias 9×1
9	Activation =Softmax	9

Table 2. Validation accuracy and validation loss f 3D-CNN-Bi-LSTM

Epoch	Iteration	Mini-batch Accuracy	Validation Accuracy	Mini-batch Loss	Validation | Loss	Base Learning Rate
1	1	4.63%	36.25%	2.7718	1.0000e-04	1.0000e-04
5	50	36.13 %.	----	1.9134	---	1.0000e-04
10	100	52.00 %	52.36%	1.2267	1.3463	1.0000e-04
14	150	65.50 %	----	0.9721	----	1.0000e-04
19	200	71.75 %	64.73%	0.7697	1.2663	1.0000e-04
23	250	81.88 %	---	0.5128	---	1.0000e-04
28	300	81.75 %	66.01%	0.5128	1.2030	1.0000e-04
32	350	87.75 %	---	0.4112	---	1.0000e-04
37	400	89.00 %	64.54%	0.3213	1.1812	1.0000e-04
41	450	91.00 %	--	0.3213	--	1.0000e-04
46	500	94.46 %	66.99%	0.2962	1.1330	1.0000e-04
50	550	98.81 %	71.12%	0.2669	1.1106	1.0000e-04

In Table III, the proposed method is compared to other classification methods such as SVM, SVM-GC, MLRsub, SVM-3D, SVM-3DG, CNN, CNN-MRF, 3D-CNN and 3D-CNN-MRF, respectively [22]. The original CNN is a plain network whose extraction layers consist of regular convolutional layers and max-pooling layers. If we use raw HSI data, DTICF is applied. These features are used for reducing the computational time. Classification results are validated in terms of OA. In Figure 6, our RGB channel assimilation of the DTICF-3D-CNN-BiLSTM-MRF approach provides the best result compared with other methods.

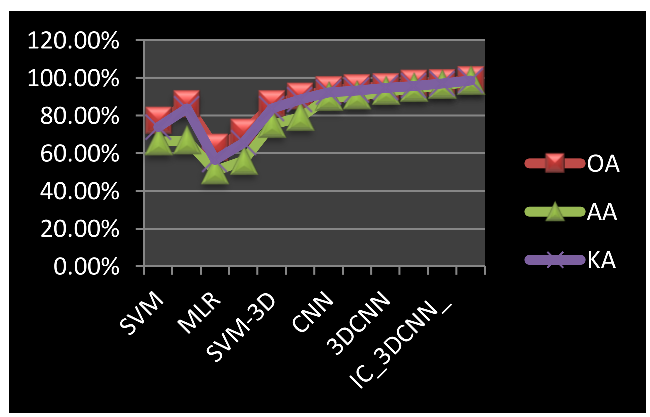

Fig. 6 Classification accuracy of the proposed method and other classification methods on the Indian pines dataset

Table 3. Overall, Average And Individual Class Accuracies (%) And Kappa Statistics Of All Competing Methods On The Indian Pines Image Test Set

Class	SVM	SVM-GC	MLR sub	MLRsub MLL	SVM-3D	SVM-3DG	CNN	CNN_MRF	3DCNN	3DCNN_MRF	IC_3DCNN_BiLSTM	IC_3DCNN_BiLSTM_MRF
1	46.34%	47.12%	27.78%	22.22%	19.51%	20.11%	34.15%	31.71%	69.69%	78.32%	93.23%	91.05%
2	69.03%	86.23%	45.36%	56.22%	82.96%	88.33%	89.57%	89.57%	89.11%	90.37%	91.20%	96.81%
3	53.41%	55.82%	18.07%	73.80%	69.21%	67.47%	88.62%	90.36%	91.98%	91.88%	92.95%	98.76%
4	15.96%	13.15%	25.93%	51.85%	61.50%	66.67%	95.12%	98.12%	97.92%	99.13%	98.68%	98.85%
5	89.63%	93.09%	71.76%	80.83%	94.93%	94.01%	94.01%	94.93%	96.27%	95.29%	96.20%	99.12%
6	97.72%	99.70%	95.55%	99.49%	98.02%	98.33%	95.59%	95.74%	94.09%	96.08%	96.18%	98.18%
7	36.00%	36.00%	18.18%	18.18%	56.00%	56.50%	76.00%	76.00%	79.37%	77.04%	88.52%	93.75%
8	98.60%	100.00%	98.95%	100.00%	100.00%	100.00%	98.84%	98.84%	98.59%	99.89%	99.18%	98.63%
9	0.00%	0.00%	0.00%	0.00%	27.78%	28.12%	100.00%	100.00%	99.64%	100.00%	98.38%	99.92%
10	65.33%	81.12%	30.63%	42.21%	75.74%	81.01%	91.99%	94.15%	93.84%	95.90%	92.09%	98.64%
11	84.16%	95.02%	85.03%	97.05%	90.18%	97.24%	95.07%	96.42%	89.97%	97.73%	98.39%	97.72%
12	68.48%	90.99%	23.84%	48.95%	82.55%	92.68%	87.43%	89.49%	91.87%	94.21%	92.20%	99.61%
13	94.57%	98.37%	93.90%	100.00%	94.57%	96.74%	98.37%	99.46%	98.65%	100.00%	98.84%	99.05%
14	98.51%	99.47%	99.01%	100.00%	96.49%	99.74%	97.98%	98.07%	98.06%	99.46%	98.31%	98.74%
15	44.38%	55.91%	7.47%	12.66%	72.91%	84.73%	89.91%	92.22%	95.02%	96.30%	97.04%	99.50%
16	93.98%	97.59%	68.92%	74.32%	84.34%	87.95%	98.80%	98.80%	99.25%	99.55%	99.12%	99.86%
OA	77.29%	85.93%	63.03%	70.88%	85.88%	89.99%	93.50%	94.62%	95.24%	96.75%	97.36%	98.82%
AA	66.01%	66.70%	50.65%	55.82%	75.42%	79.18%	89.65%	90.26%	92.71%	94.45%	96.16%	98.05%
KA	73.79%	83.72%	56.46%	65.50%	83.77%	88.46%	92.28%	93.40%	94.67%	95.82%	96.97%	98.61%

Table 4. Overall, average and individual class accuracies (%) and kappa statistics of all competing and proposed methods on the Pavia university image test set.

class	SVM	SVM-GC	MLRsub	MLRsubMLL	SVM-3D	SVM-3DG	CNN	CNN_MRF	3DCNN	3DCNN_MRF	IC_3DCNN_BiLSTM	IC_3DCNN_BiLSTM_MRF
1	74.78%	96.89%	42.72%	87.07%	92.13%	97.03%	96.78%	97.92%	97.8%	98.15%	98.54%	99.29%
2	69.75%	84.82%	69.31%	96.97%	92.70%	95.05%	96.92%	97.38%	95.83%	96.85%	97.27%	98.30%
3	71.54%	86.69%	65.57%	77.27%	79.16%	81.98%	85.96%	87.66%	91.92%	92.09%	94.22%	95.92%
4	92.79%	94.18%	86.34%	83.90%	61.50%	96.00%	98.78%	98.97%	97.31%	97.55%	98.46%	98.71%
5	96.86%	97.47%	99.16%	99.54%	94.74%	99.62%	99.92%	99.92%	98.38%	99.07%	99.04%	99.27%
6	67.27%	96.31%	56.66%	99.40%	82.20%	93.57%	90.10%	92.00%	95.7%	96.42%	97.17%	98.13%
7	75.43%	91.40%	86.20%	94.50%	87.36%	90.62%	84.42%	85.27%	89.14%	89.72%	91.36%	94.81%
8	67.68%	91.93%	65.98%	64.83%	86.05%	91.21%	89.84%	91.54%	96.31%	96.72%	97.74%	99.07%
9	98.13%	99.34%	99.67%	99.78%	100.00%	100.00%	96.80%	97.13%	99.38%	99.43%	99.49%	99.68%
OA	73.41%	90.36%	66.52%	91.13%	90.50%	92.35%	90.50%	95.68%	94.37%	97.33%	97.93%	98.67%
AA	79.36%	93.24%	74.62%	89.25%	90.44%	93.90%	90.44%	94.20%	95.76%	96.22%	97.03%	98.13%
KA	66.23%	87.52%	57.75%	88.19%	87.46%	92.60%	87.46%	94.26%	93.26%	96.69%	97.33%	98.01%

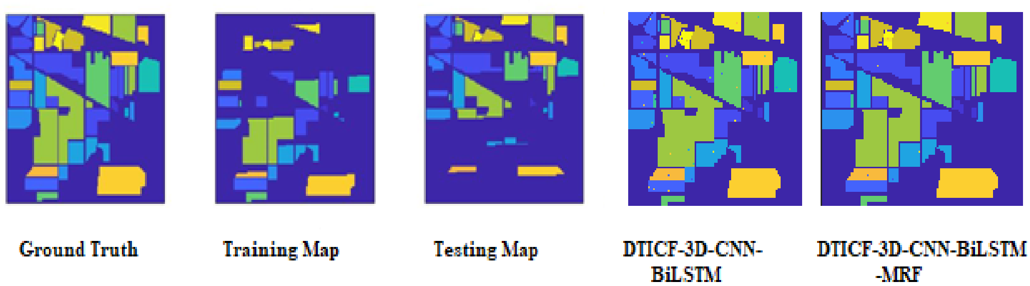

Fig. 7 Classification results obtained by DTICF-3D-CNN-BiLSTM-MRF on the Indian Pines dataset

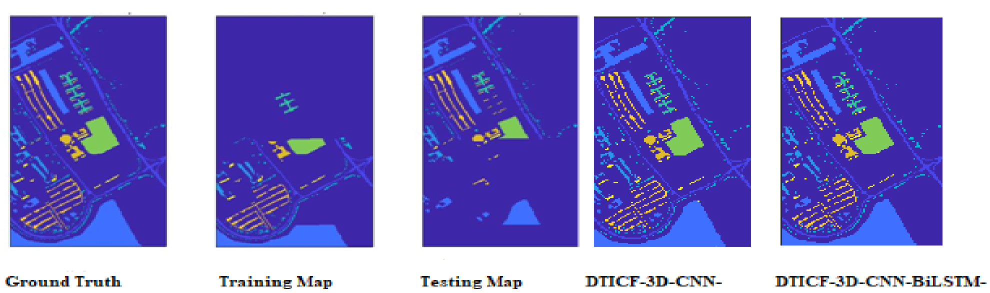

Fig. 8 Classification Result by DTICF-3D-CNN-BiLSTM-MRF on the Pavia University dataset

In our proposed work, the Indian Pines dataset is used. This dataset has high dimensionality that is difficult to classify. Figure 7 shows the classification results compared with other different methods with the help of OA scores. Compared to another classification accuracy, the proposed method DTICF-3D-CNN-BiLSTM with MRF has shown good classification performance. In Figure 4 of Indian pines, the classification accuracy of SVM-3D and SVM-3DG is 85.88% and 89.99%. The classification accuracy of CNN and CNN-MRF is 93.50% and 94.62%. The classification accuracy of 3D-CNN and 3D-CNN-MRF is 95.24% and 96.75% larger than that of CNN and CNN-MRF. Finally, the classification accuracy of DTICF-3D-CNN-BiLSTM obtains a second higher performance in the accuracy. Compared to other methods, the proposed method (98.82%) achieves the highest accuracy for HSI Classification. To examine the proposed method, Pavia university data is used. Table IV discuss the classification results compared to the other 11 classification methods. The proposed approach of DTICF-3D-CNN-BiLSTM-MRF achieved the elegant result, with a 98.67% overall delicacy, 0.36% better than another method (97.93%) achieved by DTICF-3D-CNN-BiLSTM. Figure 8 show that our proposed method provides good classification accuracy.

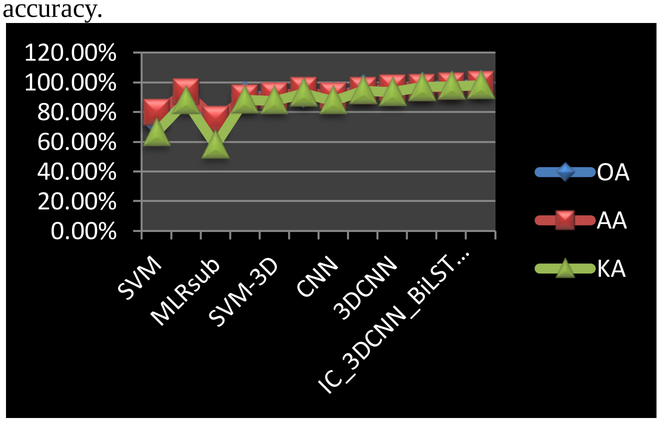

Fig. 9 Classification Accuracy of Proposed method and other classification methods on Pavia University dataset

The classification result of different methods is illustrated in Fig. 9. The above figure shows that the proposed methods achieve better classification performance compared approaches to other approaches. In Figure 6 of Pavia university's data, the classification accuracy of SVM-3D and SVM-3DG is 90.50% and 92.35%. In addition, the classification accuracy of CNN and CNN-MRF is 90.50% and 95.68%, and the classification accuracy of 3D-CNN and 3D-CNN-MRF is 94.37% and 97.33%. Finally, the classification accuracy of DTICF-3D-CNN-BiLSTM obtains a second higher performance in the accuracy. Compared to other methods, the proposed method (98.67%) achieves the highest accuracy for HSI Classification.

VI. CONCLUSION

To improve the HSI classification, the proposed RGB Channel Assimilation of 3D-CNN-BiLSTM framework has been proposed that is employed to extract the features of spectral-spatial information in this work. HSI data is converted to RGB images with spatial features. DTICF is applied to the combination of the RGB image with spatial features and raw HSI data. The excerpted features are provided to the 3D-CNN-BiLSTM. The colour features are given to 2D-CNN. The probabilistic classification map of 3D-CNN-BiLSTM and 2D-CNN is fused. Finally, MRF is utilized to improve the features map for smoothing the classification result. The proposed RGB Channel Assimilation of DTICF-3D-CNN-BiLSTM-MRF approach compared with other HSI classification methods. The experimental result clearly viewed that RGB Channel Assimilation of DTICF-3D-CNN-BiLSTM-MRF based HSI classification attained the welfare classification accuracy. In future work, we will concentrate on how to reduce computational time across a variety of HSI datasets.

REFERENCES

[1] Bandos T, Bruzzone L, and Camps-Valls G, Classification of Hyperspectral Images with Regularized Linear Discriminant Analysis, IEEE Transactions on Geoscience and Remote Sensing. 47(3) (2009) 862–873.

[2] Chen Y, Lin Z, Zhao X, Wang G, and Gu Y, Deep Learning-Based Classification of Hyperspectral Data, IEEE Journal of Topics in Applied Earth Observations and Remote Sensing. 7(6) (2014) 2094–2107.

[3] Chen Y, Nasrabadi N.M, and Tran T.D, Hyperspectral Image Classification via Kernel Sparse Representation, IEEE Transactions on Geoscience and Remote Sensing. 51(1) (2013) 217–231.

[4] Dalla Mura M, Villa A, Benediktsson J.A, Chanussot J, and Bruzzone L, Classification of Hyperspectral Images by Using Extended Morphological Attribute Profiles and Independent Component Analysis, IEEE Geoscience and Remote Sensing Letters. 8(3) (2011) 542–546.

[5] Ellis D.M, Draper N.P, and Smith H.S, Applied Regression Analysis, Applied Statistics. 17(1) (2014) 83-90.

[6] Fauvel M, Benediktsson J, Chanussot J, and Sveinsson J, Spectral and Spatial Classification of Hyperspectral Data Using SVMS and Morphological Profiles, IEEE Transactions on Geoscience and Remote Sensing. 46(11) (2008) 3804–3814.

[7] Guo Y, Cao H, Han S, Sun Y, and Bai Y, Spectral-Spatial Hyperspectral Image Classification with K-Nearest Neighbor and Guided Filter, IEEE Access. 6 (2018) 18582–18591.

[8] Haokui Zhang, Ying Li, Yenan Jiang, Peng Wang, Qiang Shen, and Chunhua Shen, Hyperspectral Classification Based on Lightweight 3-D-CNN with Transfer Learning, IEEE Transactions on Geoscience and Remote Sensing. 57(8) (2019) 5813-5830.

[9] He K.M, Sun J, and Tang X.O, Guided Image Filtering, IEEE Trans. Pattern Anal. Mach. Intell. 35(6) (2013) 1397–1409.

[10] Hochreiter S, and Schmidhuber J, Long Short-Term Memory, Neural Computation. 9(8) (1997) 1735-1780.

[11] Hughes G.F, On the Mean Accuracy of Statistical Pattern Recognizers, IEEE Transaction Information Theory. 14(1) (1968) 55-63.

[12] Hu W, Huang Y, Li W, Zhang F, and Li D.H, Deep Convolutional Neural Networks for Hyperspectral Image Classification, Journal of Sensors. 501 (2015) 258619.

[13] Jia S, Shen L, Zhu J, and Li Q, A 3-D Gabor Phase-Based Coding and Matching Framework for Hyperspectral Imagery Classification, IEEE Transactions on Cybernetics. 48(4) (2018) 1176–1188.

[14] Jun Li, and Jose M. Bioucas, Spectral- Spatial Hyperspectral Image Segmentation Using Subspace Multinomial Logistic Regression and Markov Random Fields, IEEE. 50(3) (2012).

[15] Kang X, Li S, and Benediktsson J.A, Feature Extraction of Hyperspectral Images with Image Fusion and Recursive Filtering, IEEE Transactions on Geoscience and Remote Sensing. 52(6) (2014) 3742–3752.

[16] Konstantinos Makantasis, Konstantinos Karantzalos, and Anastasios Doulamis, Deep Supervised Learning for Hyperspectral Data Classification through Convolutional Neural Networks, IEEE. (2015) 4959- 4962.

[17] Landgrebe D.A, Hyperspectral Image Data Analysis, IEEE Signal Process, Mag. 1053(5888) (2002) 17-28.

[18] Licciardi G, Marpu P.R, Chanussot J, and Benediktsson J.A, Linear Versus Nonlinear PCA for the Classification of Hyperspectral Data Based on the Extended Morphological Profiles, IEEE Geoscience and Remote Sensing Letters. 9(3) (2012) 447–451.

[19] Li J, Bioucas-Dias J.M, and Plaza A, Semisupervised Hyperspectral Image Segmentation Using Multinomial Logistic Regression with Active Learning, IEEE Transactions on Geoscience and Remote Sensing. 48(11) (2010) 4085–4098.

[20] Li J, Bioucas-Dias J.M, and Plaza A, Spectral–Spatial Hyperspectral Image Segmentation Using Subspace Multinomial Logistic Regression and Markov Random Fields, IEEE Transactions on Geoscience and Remote Sensing. 50(3) (2012) 809–823.

[21] Li J, Bioucas-Dias J.M, and Plaza A, Hyperspectral Image Segmentation Using New Bayesian Approach with Active Learning, IEEE Transactions on Geoscience and Remote Sensing. 49(10) (2011) 3947-3960.

[22] Li Y, Zhang H, and Shen Q, Spectral-Spatial Classification of Hyperspectral Imagery with 3d Convolutional Neural Network, Remote Sens. 9 (2017) 67-74.

[23] Lin Zhu, Yushi Chen and Pedram Ghamisi, Generative Adversarial Networks for Hyperspectral Image Classification, IEEE Transactions on Geoscience and Remote Sensing. 56(6) (2018) 5046 – 5063.

[24] Liu Q, Feng Z, Hang R, and Yuan X, Bidirectional-Convolutional LSTM Based Spectral-Spatial Feature Learning for Hyperspectral Image Classification, Remote Sens. 9 (2017) 1330-1340.

[25] Mandic D.P, and Chambers J, Recurrent Neural Networks for Prediction: Learning Algorithms, Architectures and Stability, John Wiley & Sons, Inc. (2001) 1-14.

[26] Melani F, and Bruzzone L, Classification of Hyperspectral Remote Sensing Images with Support Vector Machines, IEEE Transactions on Geoscience and Remote Sensing. 42(8) (2004) 1778–1790.

[27] Oliveira M.M, and Gastal E.S, Domain Transform for Edge-Aware Image and Video Processing, ACM Transactions on Graphics (Tog), ACM. 30(4) (2011) 69.

[28] Qin Xu, Yong Xiao, Dongyue Wang and Bin Luo, CSA-MSO3DCNN: Multiscale Octave 3D-CNN with Channel and Spatial Attention for Hyperspectral Image Classification, Remote Sens. (2020).

[29] Radhesyam Vaddi, and Prabukumar Manoharan, Hyperspectral Image Classification Using CNN with Spectral and Spatial Features Integration, Infrared Physics and Technology, Elsevier. 107 (2020).

[30] Shaohui Mei, Jingyu Ji, Qianqian Bi, Junhui Hou, and Qian Du, Integrating Spectral and Spatial Information into Deep Convolutional Neural Networks for Hyperspectral Classification, IEEE. (2016) 5067- 5070.

[31] Shen L, and Jia S, Three-Dimensional Gabor Wavelets for Pixel-Based Hyperspectral Imagery Classification, IEEE Transactions on Geoscience and Remote Sensing. 49(12) (2011) 5039–5046.

[32] Shi X, Chen Z, Wang H, Yeung D.Y, Wong W.K, and Woo W.C, Convolutional LSTM Network: A Machine Learning Approach for Precipitation Nowcasting, Advances in Neural Information Processing Systems. 28 (2015) 1049–5258. [Online]. Available: www.Papers.Nips.Cc/Paper/5955-Convolutional-Lstm-Networka-Machine-Learning-Approach-For-Precipitation-Nowcasting

[33] Sun X, Qu Q, Nasrabadi N. M, and Tran T. D, Structured Priors for Sparse-Representation-Based Hyperspectral Image Classification, IEEE Geoscience and Remote Sensing Letters. 11(7) (2014) 1235–1239.

[34] Szegedy C, Toshev A, and Erhan D, Deep Neural Networks for Object Detection, In Advances in Neural Information Processing Systems. (2013) 2553–2561.

[35] Yushi Chen, Chouhan Lin And Xing Zhao, Deep Learning-Based Classification of Hyperspectral Data, IEEE Journal of Selected Topics in Applied Earth Observations and Remote Sensing, IEEE. 7(6) (2014) 2094-2107.